AGU PUBLICATIONS

JGR

Journal of Geophysical Research: Solid Earth

RESEARCH ARTICLE

10.1002/2013JB010583

Key Points:
- Seismicity along the CVL is focused around Mount Cameroon
- CVL magmatism has had little impact on the overlying lithosphere
- Lithospheric delamination is an appropriate candidate for CVL development

Correspondence to:
I. D. Bastow,
i.bastow@imperial.ac.uk

Citation:
De Plaen, R. S. M., I. D. Bastow, E. L. Chambers, D. Keir, R. J. Gallacher, and J. Keane (2014), The development of magmatism along the Cameroon Volcanic Line: Evidence from seismicity and seismic anisotropy, *J. Geophys. Res. Solid Earth*, *119*, 4233–4252, doi:10.1002/2013JB010583.

Received 6 AUG 2013
Accepted 11 APR 2014
Accepted article online 15 APR 2014
Published online 8 MAY 2014

The development of magmatism along the Cameroon Volcanic Line: Evidence from seismicity and seismic anisotropy

R. S. M. De Plaen[1,2], I. D. Bastow[3], E. L. Chambers[4], D. Keir[4], R. J. Gallacher[4], and J. Keane[3]

[1]School of Earth Sciences, University of Bristol, Bristol, UK, [2]Now at Faculty of Science, Technology and Communication, University of Luxembourg, Luxembourg City, Luxembourg, [3]Department of Earth Science and Engineering, Imperial College London, London, UK, [4]National Oceanography Centre Southampton, University of Southampton, Southampton, UK,

Abstract The Cameroon Volcanic Line (CVL) straddles the continent-ocean boundary in West Africa but exhibits no clear age progression. This renders it difficult to explain by traditional plume/plate motion hypotheses; thus, there remains no consensus on the processes responsible for its development. To understand better the nature of asthenospheric flow beneath the CVL, and the effects of hotspot tectonism on the overlying lithosphere, we analyze mantle seismic anisotropy and seismicity. Cameroon is relatively aseismic compared to hotspots elsewhere, with little evidence for magmatism-related crustal deformation away from Mount Cameroon, which last erupted in 2000. Low crustal V_p/V_s ratios (~1.74) and a lack of evidence for seismically anisotropic aligned melt within the lithosphere both point toward a poorly developed magmatic plumbing system beneath the CVL. Null *SKS* splitting observations dominate the western continental portion of the CVL; elsewhere, anisotropic fast polarization directions parallel the strike of the Precambrian Central African Shear Zone (CASZ). The nulls may imply that the convecting upper mantle beneath the CVL is isotropic, or characterized by a vertically oriented olivine lattice preferred orientation fabric, perhaps due to a mantle plume or the upward limb of a small-scale convection cell. Precambrian CASZ fossil lithospheric fabrics along the CVL may have been thermomechanically eroded during Gondwana breakup ~130 Ma, with an isotropic lower lithosphere subsequently reforming due to cooling of the slow-moving African plate. Small-scale lithospheric delamination during the 30 Ma recent development of the line may also have contributed to the erosion of the CASZ lithospheric fossil anisotropy, at the same time as generating the low-volume alkaline basaltic volcanism along the CVL.

1. Overview

The Cameroon Volcanic Line (CVL) lies to the north of the Congo Craton in West Africa and straddles the continent-ocean boundary (Figure 1). Unlike Hawaii, the archetypal example of a linear hotspot chain, the CVL displays no clear age progression along its length [e.g., *Fitton and Dunlop*, 1985; *Fitton*, 1987; *Poudjom Djomani et al.*, 1997], thus rendering it difficult to explain by the traditional idea of a plate moving over a relatively stationary hotspot [e.g., *Morgan*, 1983]. Africa's very slow movement NW since ~30 Ma [e.g., *Steinberger and Torsvik*, 2008] may contribute to the longevity and lack of age progression along the CVL, but the paucity of detailed constraints on the upper mantle structure beneath the region means the causative mechanism(s) for the volcanic line remains uncertain. The nature of the magmatic plumbing system along the CVL also remains poorly constrained. Petrological studies indicate that the CVL's mostly alkaline basaltic volcanoes have erupted relatively low volumes of igneous rocks [e.g., *Fitton*, 1980; *Suh et al.*, 2003]. These silica-poor lavas have not undergone appreciable fractionation at depth, which raises the question of whether or not the crust beneath the CVL is characterized by cooled mafic intrusions and/or present-day melt, as is often observed elsewhere at continental hotspots and rifts worldwide [e.g., *Maguire et al.*, 2006; *Thybo and Nielsen*, 2009].

Several models have been proposed to explain the development of the CVL. These can be grouped as plume and nonplume based. The plume-based models range from a single plume under a moving plate [e.g., *Burke*, 2001; *Lee et al.*, 1994; *Morgan*, 1983; *Van Houten*, 1983] to multiple plumes [e.g., *Ngako et al.*, 2006] beneath the region. It has also been suggested that lateral flow of buoyant asthenosphere from the Afar hotspot in East Africa may now be contributing to the volcanism along the CVL [*Ebinger and Sleep*, 1998]. Nonplume models include decompression melting beneath reactivated shear zones in Cameroon

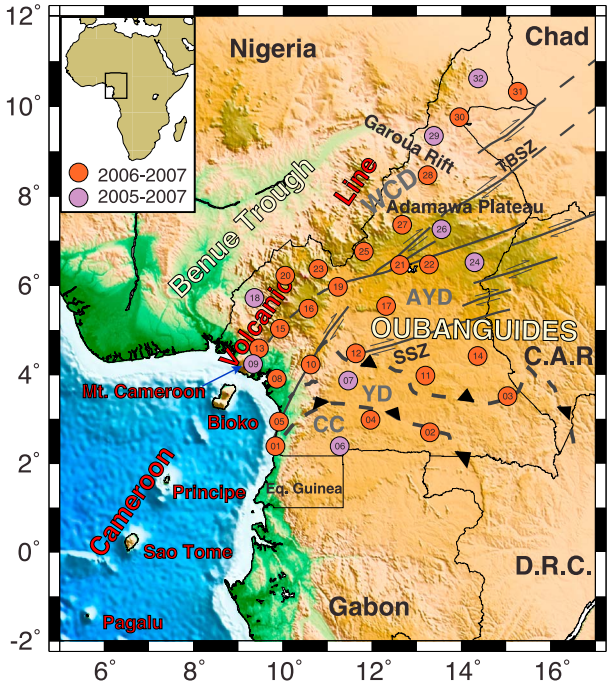

Figure 1. Topographic map of Cameroon showing the locations of Cameroon Broadband Seismic Experiment (CBSE) seismograph stations. Numbers are station codes (Table 1). Also shown are major geologic features [e.g., *Toteu et al.*, 2004; *Nzenti et al.*, 2006; *Reusch et al.*, 2010] such as the CVL and the Benue Trough. CC: Congo Craton (Archean), the features north of which are parts of the Oubanguides belt. Heavy dashed lines are thrust faults. The domains are modified from *Toteu et al.* [2004] and *Nzenti et al.* [2006]. YD: Yaounde Domain (Neoproterozoic), AYD: Adamawa-Yade Domain (Paleoproterozoic), and WCD: Western Cameroon Domain (Neoproterozoic). Heavy black lines are major strike-slip faults of the Central African Shear Zone as defined by *Ngako et al.* [2003], *Toteu et al.* [2004], and *Nzenti et al.* [2006]. SSZ: Sanaga Shear Zone and TBSZ: Tchollir-Banyo Shear Zone.

[*Fairhead*, 1988; *Fairhead and Binks*, 1991], or small-scale mantle convection [e.g., *Meyers et al.*, 1998; *King and Anderson*, 1998; *King*, 2007] in the zone between two deeply rooted cratons that was reactivated during the Mesozoic breakup of Gondwana. *Milelli et al.* [2012] and *Fourel et al.* [2013] use scaled laboratory models and analytical solutions to investigate lithospheric instabilities in the vicinity of large lateral variations in lithospheric thickness, as is observed along the CVL between the deeply rooted West African and Congo Cratons, and the continent-ocean boundary. These models suggest that lithospheric instabilities at the edge of a continent can develop over long timescales, leading to small rates of upwelling and decompression melting along linear zones, as is observed in Cameroon.

Each of the aforementioned scenarios for CVL development predicts different patterns of mantle flow, which in turn are expected to be manifested as seismic anisotropy, measurable via analysis of shear wave splitting [e.g., *Silver and Chan*, 1991], as outlined below. Olivine is the most abundant mineral in the upper mantle and is highly anisotropic. Strain results in development of crystallographic preferred orientation of olivine, leading to alignment of *a* axes in the flow direction [e.g., *Zhang and Karato*, 1995; *Bystricky et al.*, 2000; *Tommasi et al.*, 2000]. If a shear wave travels through such a medium, the faster traveling component will travel parallel to the *a* axes of the crystal [e.g., *Silver and Chan*, 1991]. Shear wave splitting parameters ϕ (the orientation of the fast shear wave) and δt (the lag time between the fast and slow shear wave) can therefore be related, for example, to asthenospheric flow [e.g., *Vinnik et al.*, 1989; *Fouch et al.*, 2000; *Sleep et al.*, 2002], the preferential alignment of fluid or melt [e.g., *Blackman and Kendall*, 1997], preexisting anisotropy frozen in the lithosphere [e.g., *Silver and Chan*, 1988; *Vauchez and Nicolas*, 1991; *Bastow et al.*, 2007], or any combination thereof. In the case of Cameroon, vertically aligned olivine in a mantle plume or the upward/downward limb of a small-scale convection cell would be expected to be manifested as near-zero splitting in *SKS* phases. In contrast, horizontal asthenospheric flow from the Afar hotspot would be manifested as marked shear wave splitting in *SKS* phases, with the fast shear wave polarization direction parallel to the direction of flow. Lithospheric fossil anisotropy would be expected to parallel trends of major faults or rock fabrics, lithospheric thickness variations, or trends inferred from potential field data such as gravity and magnetics.

In this study, we perform shear wave splitting analysis of *SKS* phases recorded by the recent Cameroon Broadband Seismic Experiment (CBSE) [e.g., *Reusch et al.*, 2010; *Tokam et al.*, 2010] to investigate upper mantle anisotropy beneath the CVL and the edge of the neighboring Congo Craton. These constraints on mantle anisotropy allow us to explore the extent to which the assembly and subsequent breakup of Gondwana has imparted a fossil anisotropic fabric on the Cameroon lithosphere. By constraining the directionality of the flowing asthenosphere beneath the CVL, we are also able to discriminate between competing models for its development. If the lithospheric magmatic plumbing system of the CVL is characterized by large volumes

of partial melt, aligned within SE-NW striking faults and fractures of the Central African Shear Zone (CASZ), this too will be manifested as strong seismic anisotropy. A study of seismicity along the CVL also provides an opportunity to examine the extent to which ongoing magmatism along the line is manifested as seismic activity: a common feature at hotspots such as Iceland [e.g., *Key et al.*, 2011] and Ethiopia [e.g., *Ebinger et al.*, 2010], and at hotspots in intraplate settings such as Galapagos and Hawaii [*Tepp et al.*, 2014], where fluid migration is ongoing.

2. Geology and Tectonic Setting

Cameroon comprises several tectonic domains brought together during the Pan-African Cycle ~600 Ma [*Djomani et al.*, 1995]. The Oubanguides Belt (Figure 1) is a part of the larger Neoproterozoic Pan-African-Brazilian Belt created during the formation of Gondwana with the collision of the São Francisco Craton, the Congo Craton, and the West African Craton [e.g., *Castaing et al.*, 1994; *Ngako et al.*, 2003; *Toteu et al.*, 2004]. To the north of the Congo Craton, three main tectonic units are identified: the Neoproterozoic Yaounde Domain, the Paleoproterozoic Adamawa-Yade Domain, and the Neoproterozoic Western Cameroon Domain (Figure 1). The domain boundaries are defined by large shear zones such as the Sanaga Shear Zone and the Tchollir-Banyo Shear Zone (TBSZ), which form part of the larger Precambrian Central African Shear Zone (CASZ), which extends across the African continent from the Darfur region of Sudan, through Central Africa, to the Adamawa Plateau in Cameroon [e.g., *Toteu et al.*, 2004; *Nzenti et al.*, 2006; *Castaing et al.*, 1994]. The Pernambuco lineament in Brazil is probably the extension of the shear zone on the conjugate Atlantic-rifted margin [e.g. *Dorbath et al.*, 1986; *Djomani et al.*, 1995]. The opening of the South Atlantic during Cretaceous times (beginning ~130 Ma) signaled the breakup of Gondwana with at least partial reactivation of strike-slip faults along the CASZ producing narrow subsiding rift basins infilled with Cretaceous-Tertiary sediments [e.g. *Fairhead*, 1988]. Geological studies along the CASZ estimate ≥40 km of dextral displacement [see, e.g., *Daly et al.*, 1989]. Mesozoic rifting also resulted in the formation of a series of major basins and grabens, such as the Benue Trough, to the west of the CVL (Figure 1) [e.g., *Djomani et al.*, 1995].

The Cenozoic CVL trends N30°E and extends from Pagalu Island to northernmost Cameroon (Figure 1). Volcanic activity along the CVL had begun on the continental and oceanic sectors by ~30 Ma [e.g., *Déruelle et al.*, 2007]. Erosion has exposed more than 60 anorogenic ring complexes on the continental sector, ranging in age from 6 to 70 Myr [e.g., *Montigny et al.*, 2004; *Déruelle et al.*, 2007]. By late Eocene/early Oligocene times volcanism had spread along the entire line, but without any clear age progression during its development [e.g., *Fitton and Dunlop*, 1985; *Fitton*, 1987; *Poudjom Djomani et al.*, 1997]. Most volcanic centers have been active in the past million years, though Mount Cameroon at the center of the line is the only one with a historically recorded eruption (in the year 2000) [e.g., *Suh et al.*, 2003; *Déruelle et al.*, 2007].

Igneous rocks along the CVL are mostly of alkaline basalt composition, and their isotopic and chemical composition is very similar in both the continental and the oceanic sectors [*Fitton and Dunlop*, 1985; *Fitton*, 1987]. This has been cited as evidence for a single source of volcanism beneath the CVL [e.g. *Halliday et al.*, 1988; *Rankenburg et al.*, 2005; *Déruelle et al.*, 2007]. Numerous petrological studies indicate that the CVL's volcanoes have mostly erupted low volumes of alkaline melt rapidly, with little-to-no fractionation within the crust during ascent to the surface. Thus, melt is being sourced almost directly from the mantle [e.g., *Fitton and Dunlop*, 1985; *Fitton*, 1987; *Marzoli et al.*, 2000; *Suh et al.*, 2003; *Déruelle et al.*, 2007]. The nature and extent of these lithospheric-scale conduits, however, remains elusive.

3. Geophysical Constraints

Mantle structure beneath Cameroon is shown in many global tomographic studies to be seismically slow [e.g., *Montelli et al.*, 2006; *Ritsema et al.*, 2011]. This is corroborated by observations from continent-scale surface wave studies [*Pasyanos and Nyblade*, 2007; *Priestley et al.*, 2008; *Fishwick*, 2010] that also indicate that the CVL mantle is characterized by slow seismic wave speeds. The lithosphere-asthenosphere boundary is <100 km deep beneath the CVL, which in turn lies to the south of a failed continental rift zone (the Benue Trough). Beneath the neighboring Congo and West African Cratons, the lithosphere is ~250 km thick [*Fishwick*, 2010]. A recent study by *Reusch et al.* [2011] showed that the olivine phase transitions from olivine to wadsleyite (the "410") and from ringwoodite to perovskite + magnesiowüstite (the "660") are at normal depths beneath the CVL, suggesting that any thermal anomaly beneath the CVL is confined to the upper

mantle. *Dorbath et al.* [1986] completed a teleseismic delay survey across the Adamawa Plateau, finding $\delta V_P < 2.5\%$ regional variations in seismic wave speed across the study area. More recently, *Reusch et al.* [2010] used body wave relative arrival time tomography to image the mantle seismic structure beneath the CVL. A continuous low-velocity zone ($\delta V_S = -2$ to -3%) underlies the entire CVL to a depth of at least 300 km and was attributed by *Reusch et al.* [2010] to a thermal anomaly of ≥280 K. However, studies of absolute mantle wave speed beneath Cameroon are not as low as in other hotspots worldwide. In Ethiopia, for example, surface wave studies [*Keranen et al.*, 2009; *Dugda et al.*, 2007; *Bastow et al.*, 2010] reveal wave speeds of ≤4 km s^{-1} for the Ethiopian rift: $\delta V_S \geq 11\%$ slow. In contrast, similar constraints from Cameroon indicate *S* wave speeds consistently ≥4.1 km s^{-1} beneath the CVL: $\delta V_S \leq 8\%$ slow [e.g., *Tokam et al.*, 2010].

Flow models constrained by global tomography [e.g., *Forte et al.*, 2010] predict a strong lateral mantle flow field in the asthenosphere beneath Cameroon approximately parallel to the CVL. This would be expected to be manifest as CVL-parallel seismic anisotropy due to lattice preferred orientation of mantle minerals beneath our study area. The *Forte et al.* [2010] study also predicts a strong upwelling component to the mantle flow field from a region termed the West African Superplume.

Seismic anisotropy in Cameroon has been studied via analysis of *SKS* splitting by *Koch et al.* [2012]. They identify four regions of distinct anisotropy: (1) moderately strong NE-SW oriented fast polarization directions ($\delta t \approx 1.0$ s) beneath the Congo Craton in the south, and the Garoua rift in the north (Figure 1); (2) weak anisotropy ($\delta t \approx 0.3$ s) between the Congo Craton and the CVL; (3) N-S oriented fast polarization directions within the CVL, with $\delta t \approx 0.7$ s. *Koch et al.* [2012] interpreted these observations as evidence for small-scale mantle convection beneath Cameroon.

Crustal structure in Cameroon has been investigated using both passive and active seismic sources [e.g., *Stuart et al.*, 1985; *Dorbath et al.*, 1986; *Plomerova et al.*, 1993; *Meyers et al.*, 1998; *Tokam et al.*, 2010; *Gallacher and Bastow*, 2012] and potential field studies [e.g., *Fairhead and Okereke*, 1987; *Toteu et al.*, 2004; *Tadjou et al.*, 2009] that help to constrain the lithospheric subdivisions of the region. For example, thinned crust (~25 km) is imaged beneath the Garoua Rift (Figure 1), while the transition from the CVL to the Congo Craton is characterized by a transition from ~36 km thick crust to 43–48 km thick crust [*Tokam et al.*, 2010; *Gallacher and Bastow*, 2012]. Average crustal shear wave velocity also increases into the craton from the CVL: from ~3.7 km s^{-1} to ~3.9 km s^{-1} [*Tokam et al.*, 2010]. Bulk crustal V_p/V_s ratios along the CVL are markedly low (~1.74) compared to other hotspots worldwide, an observation that *Gallacher and Bastow* [2012] cited as evidence for the lack of melt fractionation and intrusion during the ~30 Ma development of the CVL.

Gravity studies have been conducted in the region to delineate tectonic boundaries, to explore crustal thinning, and to evaluate variations in lithospheric rigidity. Most of them highlight the various major geologic and tectonic features in the region, such as the Benue Trough with a significant positive Bouguer anomaly, the Adamawa uplift with a negative anomaly [e.g., *Poudjom Djomani et al.*, 1992, 1997; *Fairhead and Okereke*, 1987] and the Congo Craton with a negative anomaly [e.g., *Poudjom Djomani et al.*, 1997; *Tadjou et al.*, 2009]. Evidence for continental collision was found at the northern margin of the Congo Craton, as well as a positive anomaly associated with the CASZ that bisects the Adamawa uplift [e.g., *Poudjom Djomani et al.*, 1997; *Tadjou et al.*, 2009]. For a recent review of broadband seismological constraints in Cameroon, see *Fishwick and Bastow* [2011].

Effective elastic plate thickness (T_e) depends on geothermal gradient, crustal composition, and crust and mantle lithospheric thickness [e.g., *Lowry and Pérez-Gussinyé*, 2011]. *Pérez-Gussinyé et al.* [2009] constrained lithospheric strength via study of T_e across the African continent using coherence analysis of topography and Bouguer anomaly data. The weakest lithosphere was found in Ethiopia, a region of incipient continental breakup characterized by a markedly low wave speed [e.g., *Bastow et al.*, 2010], hot [*Rooney et al.*, 2012; *Ferguson et al.*, 2013] mantle. Channels of relatively weak lithosphere extend across the African continent from this region to Cameroon, where T_e is also relatively low compared to the surrounding cratons. *Pérez-Gussinyé et al.* [2009] interpreted these observations as supportive of the model of *Ebinger and Sleep* [1998], who proposed that flow of buoyant upper mantle beneath continental lithosphere thinned extensively during Mesozoic rifting may now be contributing to volcanism along the CVL.

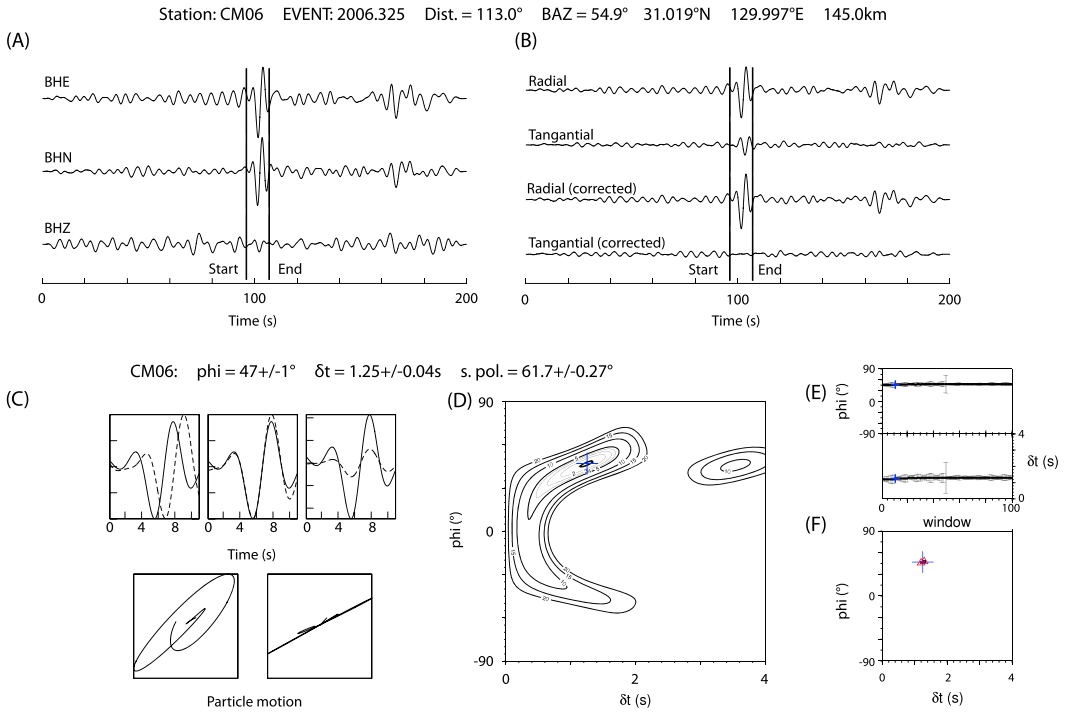

Figure 2. Example of a good shear wave splitting measurement for station CM06: (a) original three components (east, north, and vertical) of the *SKS* phase and the selection window used; (b) radial and tangential components before and after the analysis was performed; observe that energy on the tangential component has been removed; (c) match between the fast and slow waveform and the linearization of the particle motion; (d) error and uncertainty calculation, here a stable result and a well constrained 95% confidence contour (thick line) indicate a robust measurement; (e) measurements of ϕ and δt obtained from 100 different analysis windows plotted against window number; (f) cluster analysis of splitting parameters obtained from the 100 windows. Good results are stable over a large number of windows.

4. Data and Analysis

4.1. Shear Wave Splitting

Data in this study come from the CBSE network of 32 portable broadband seismometers spaced 50–150 km apart across the CVL and the western edge of the neighboring Congo Craton (Figure 1) [e.g., *Reusch et al.*, 2010; *Tokam et al.*, 2010]. The stations operated between January 2005 and February 2007. Waveforms for earthquakes of magnitude $m_b \geq 5.5$ were visually inspected for high signal-to-noise ratio *SKS* phases, with earthquakes of epicentral distances $\leq$88° eliminated from the analysis in order to prevent contamination by other shear wave phases. Data were filtered prior to analysis with a zero-phase two-pole Butterworth filter with corner frequencies of 0.04–0.3 Hz.

Traditional shear wave splitting analysis requires a single shear wave analysis window to be selected [*Silver and Chan*, 1991]. The earlier study of the CVL by *Koch et al.* [2012] adopted such an approach. The choice of a final window is somewhat subjective, however, and in many cases different windows give very different results. To overcome this problem, we adopt here the semi-automated approach of *Teanby et al.* [2004], which is based on the method of *Silver and Chan* [1991].

For *SKS* waves, elliptical particle motion and energy on the tangential component seismogram are strong evidence for shear wave splitting. We rotated and time shifted the horizontal components to minimize the second eigenvalue of the covariance matrix for particle motion of a time window around the *SKS* phase. This procedure linearizes the particle motion and usually reduces the tangential component energy (assuming that the incoming *SKS* wave is radially polarized before entering the anisotropic medium). In the *Teanby et al.* [2004] approach, the splitting analysis is performed for 100 different windows, each encapsulating the *SKS* energy. Cluster analysis is then used to find pair of splitting parameters (ϕ, δt) that are stable over many different windows, which is not necessarily the pair with the lowest errors. An example of this procedure is shown in Figure 2. In the final analysis, a database of 78 splitting measurements was assembled from 23 earthquakes (Figure 3 and Table 1).

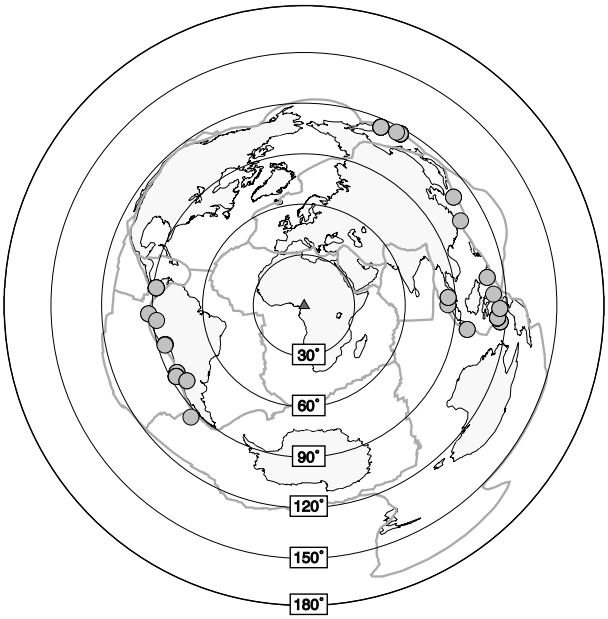

Figure 3. The global distribution of all the earthquakes used in the study plotted with an azimuthal equidistant map projection. The center of the CBSE network is marked by the triangle.

4.2. Seismicity

We analyzed seismicity in Cameroon during the period 28 January 2006 to 30 June 2006 to constrain patterns of earthquakes along the CVL. Continuous data from the Cameroon network is heavily contaminated by high-frequency cultural noise. We thus identified earthquakes on filtered seismograms, using a zero-phase Butterworth band-pass filter with corner frequencies of 0.5 and 4 Hz. *P* and *S* wave arrivals are generally emergent, and their codas contain no significant energy at frequencies higher than 4 Hz.

After waveform filtering, *P* and *S* wave arrival times were measured and used to compute earthquake locations using Hypoinverse-2000 [*Klein*, 2002] with a 1-D velocity model previously employed in the region [e.g., *Ubangoh et al.*, 1997; *Ateba and Ntepe*, 1997]. A Wadati diagram, plotted using the *P* and *S* wave local earthquake traveltimes, reveals a best fit V_p/V_s ratio of 1.74 (Figure 6)

Table 1. Hypocentral Information for Earthquakes Used in the *SKS* Splitting Analysis

Date (dd/mm/yyyy)	Time (HH:MM)	Lat/Lon (°N/°E)	Depth (km)	Stations
02/03/2005	10:42	−6.53/129.93	202	CM06, CM18, CM26, and CM32
14/05/2005	05:05	0.59/98.46	34	CM29
21/05/2005	05:11	−3.29/−80.99	40	CM18 and CM24
15/06/2005	19:52	−44.87/−80.56	10	CM09
26/06/2005	14:11	−15.35/−72.96	111	CM26 and CM29
26/09/2005	01:55	−5.68/−76.40	115	CM24
15/10/2005	15:51	25.32/123.36	183	CM07
21/11/2005	15:36	31.02/130.00	145	CM06 and CM26
30/11/2005	16:53	6.27/124.03	13	CM07 and CM18
23/01/2006	20:50	6.86/−77.79	14	CM17, CM24, CM28, and CM30
27/01/2006	16:58	−5.47/128.13	397	CM01, CM02, CM05, CM06, CM13, CM15, CM18, CM19, CM20, CM21, CM22, CM23, CM24, CM25, CM26, CM27, and CM29
01/04/2006	10:02	22.87/121.28	9	CM28
30/04/2006	21:40	−27.21/−71.06	12	CM03, CM28, and CM32
16/07/2006	11:42	−28.72/−72.54	10	CM03, CM17, CM25, CM29, and CM30
24/08/2006	21:50	51.15/157.52	43	CM01, CM03, CM07, CM10, CM11, CM16, CM18, and CM31
16/09/2006	09:45	−3.08/129.44	17	CM02, CM03, and CM12
17/09/2006	09:34	−31.75/−67.18	142	CM31 and CM32
21/09/2006	18:54	−9.05/110.36	25	CM12 and CM32
30/09/2006	16:26	−15.59/−73.16	107	CM22
30/09/2006	17:50	46.35/153.17	11	CM02, CM07, CM10, CM16, CM18, CM22, and CM32
01/10/2006	09:06	46.47/153.24	19	CM02, CM10, CM11, CM16, CM18 CM29, CM22, and CM32
15/11/2006	21:22	47.28/154.15	12	CM31
01/12/2006	03:58	3.40/99.09	206	CM01, CM05, CM10, CM15, and CM20
21/01/2007	11:27	1.07/126.28	22	CM12 and CM17

Table 2. Shear Wave Splitting Parameters (Fast Polarization Direction, ϕ; Delay Time, δt) Are From the CBSE Network[a]

Station (*N*)	Station Lat/Lon (°N/°E)	ϕ (deg)	σ_ϕ (deg)	δt (s)	$\sigma_{\delta t}$ (s)	Event Lat/Lon (°N/°E)	BAZ (deg)
CM02	2.70/13.29	47	8	1.25	0.10	−3.08/129.44	92.09
		46	3	1.08	0.03	−5.47/128.13	94.75
Stacked (4)		**36**	**1**	**1.15**	**0.03**	-	-
CM05	2.94/9.91	19	12	0.60	0.18	3.40/99.09	86.67
Stacked (2)		**22**	**9**	**0.60**	**0.14**	-	-
CM06	2.38/11.27	58	10	0.85	0.11	−6.53/129.93	96.10
		47	1	1.25	0.04	31.02/130.00	54.88
		70	5	1.08	0.09	−5.47/128.13	94.90
Stacked (3)		**42**	**1**	**0.98**	**0.04**	-	-
CM10	4.22/10.62	23	5	0.70	0.09	3.40/99.09	86.75
Stacked (4)		**28**	**4**	**0.65**	**0.04**	-	-
CM12	4.48/11.63	0	1	1.95	0.06	−3.08/129.44	91.11
Stacked (3)		**2**	**1**	**1.95**	**0.09**	-	-
CM15	5.03/9.93	41	17	0.47	0.17	3.40/99.09	86.71
Stacked (2)		**47**	**16**	**0.48**	**0.13**	-	-
CM17	5.55/12.31	19	12	1.50	0.21	−28.72/−72.54	241.08
		38	3	1.63	0.08	6.86/-77.79	276.80
Stacked (3)		**30**	**4**	**1.65**	**0.11**	-	-
CM21	6.47/12.62	72	4	1.48	0.08	−5.47/128.13	92.94
Stacked (1)		**73**	**4**	**1.50**	**0.08**	-	-
CM22	6.48/13.27	54	21	0.73	0.40	−5.47/128.13	92.99
		64	15	0.75	0.18	46.35/153.17	29.89
Stacked (3)		**62**	**4**	**0.80**	**0.07**	-	-
CM24	6.52/14.29	74	4	0.70	0.11	−5.47/128.13	93.06
Stacked (4)		**76**	**4**	**0.75**	**0.13**	-	-
CM26	7.26/13.55	30	10	0.93	0.14	−6.53/129.93	93.64
		27	6	0.95	0.14	−5.47/128.13	92.65
Stacked (4)		**57**	**4**	**0.63**	**0.06**	-	-
CM27	7.36/12.67	37	12	0.75	0.13	−5.47/128.13	92.52
Stacked (1)		**38**	**12**	**0.78**	**0.13**	-	-
CM29	9.35/13.39	65	2	1.23	0.08	−15.35/−72.96	254.37
		57	3	1.08	0.03	−5.47/128.13	91.66
Stacked (5)		**63**	**1**	**1.15**	**0.03**	-	-
CM31	10.33/15.26	66	7	0.82	0.06	51.15/157.52	24.32
Stacked (3)		**64**	**2**	**0.88**	**0.09**	-	-
CM32	10.62/14.37	44	15	0.88	0.34	−31.75/-67.18	237.46
		62	11	0.82	0.12	−6.53/129.93	92.08
		69	6	1.15	0.08	−9.05/110.36	97.81
Stacked (6)		**52**	**2**	**0.93**	**0.05**	-	-

[a]Errors associated with each measurement are the σ_ϕ and $\sigma_{\delta t}$; *N* is the number of individual measurements used to constrain the stacked splitting parameters. BAZ: backazimuth. Bold text highlights the stacked results.

and this value was used for the earthquake locations. Hypocenters were only obtained for earthquakes with four or more phase readings at three or more stations. The errors associated with earthquake location vary depending on the proximity of the earthquake to the seismic network. The depth distribution of the earthquakes is shown in Figures 7 and 8.

The majority of earthquakes are concentrated in the SW corner of the study region, near Mount Cameroon and extending offshore near the island of Bioko (Figure 8). Earthquakes near Mount Cameroon are proximal to the seismic network and have estimated horizontal errors of ±1 km and vertical errors of ±2 km. Those located offshore and outside the seismic network have horizontal errors of ±5 km but vertical errors of up to ±10 km. We therefore confidently interpret the distribution of hypocenters for earthquakes located onshore and only interpret epicenter distribution for earthquakes offshore. As far as we have been able to determine, the NE area of the CVL is aseismic, though we cannot preclude the possibility that this is due to the limited station density and relatively short period of network operation.

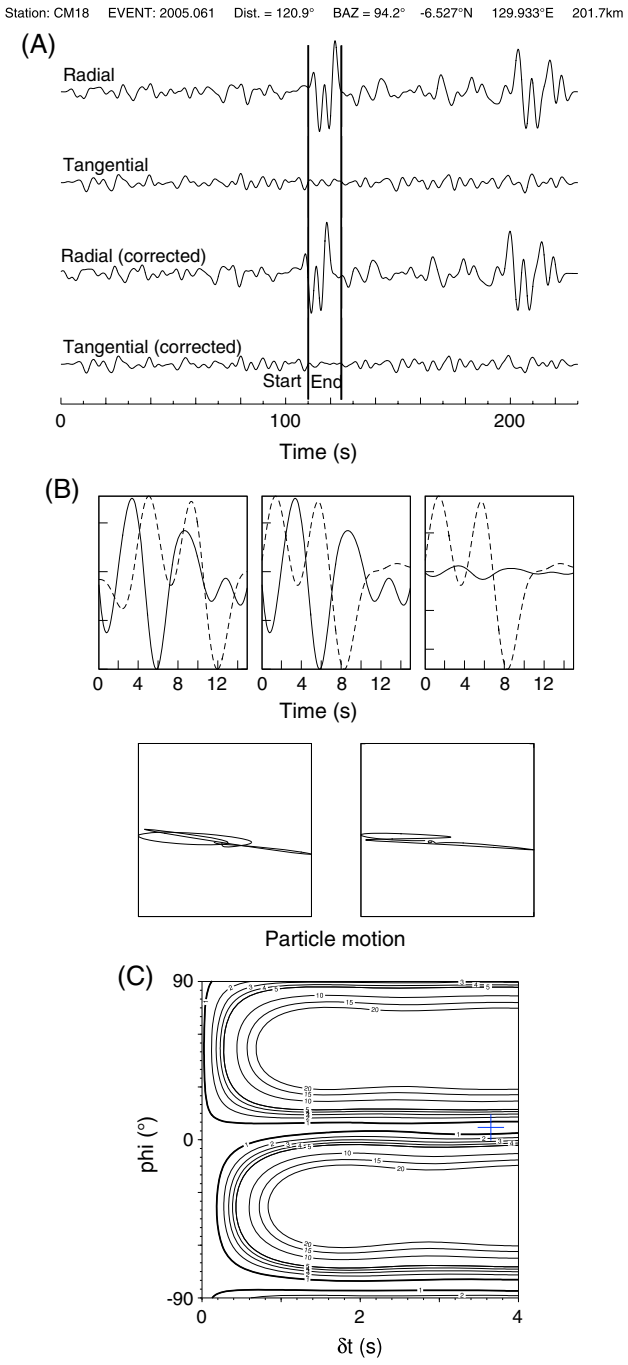

Figure 4. Example of a null measurement for station CM18. (a) There is no energy on the tangential component, and (b) the particle motion is already linear before the analysis is performed. These are evidence of the absence of splitting. The (c) stretched confidence contours are typical of a null measurement.

Local magnitudes (M_L) of the earthquakes were computed, with maximum zero-to-peak amplitude measured on simulated horizontal-component Wood-Anderson displacement seismograms after removal of instrument response [e.g., *Richter*, 1935; *Keir et al.*, 2006]. These measurements were used in conjunction with hypocentral distances to estimate M_L using the distance correction originally employed to estimate M_L in California [*Richter*, 1935]. Earthquake magnitudes are shown in Figure 8.

5. Results and Comparisons to Previous Studies

5.1. Shear Wave Splitting

Individual shear wave splitting parameters are listed in Table 2, with associated hypocentral information in Table 1. Across the CBSE network δt varies from 0.6 to 1.95 s, with several stations showing δt >1 s (Figure 5). At stations where several shear wave splitting measurements were made, no significant back azimuthal variation in ϕ or δt was observed (Table 2), with the implication that anisotropy in the mantle beneath can be approximated as a single, homogeneous, horizontal layer [e.g., *Silver and Savage*, 1994]. We thus computed single-splitting parameters for each station using the stacking method of *Restivo and Helffrich* [1999]. The final splitting data set is presented in Figure 5.

For some station earthquake pairs in our analysis, no tangential component energy was noted, and the particle motion was linear prior to shear wave splitting analysis. This implies either that the mantle beneath the station is seismically isotropic or that the incoming shear wave energy is polarized parallel to or perpendicular to the true anisotropic fast direction that characterizes the subsurface. An example of a null splitting measurement is shown in Figure 4. Stations at which only null measurements were observed were predominantly in the southern to central portions of the CVL (Figure 5 and Table 3). Elsewhere, splitting parameters vary significantly in both ϕ and δt over relatively short (50–150 km) length scales with ϕ generally NNE-ENE (Figure 5 and Table 2).

Table 4 shows a comparison of splitting parameters obtained in this study with that of *Koch et al.* [2012]. As mentioned earlier, the *Koch et al.* [2012] study identifies four regions of distinct anisotropy: (1) moderately strong NE-SW oriented fast directions ($\delta t \approx 1.0$ s) beneath the Congo Craton in the south, and the

Figure 5. Shear wave splitting parameters (blue arrows) from CBSE stations (white triangles) in Cameroon. Black crosses are null measurements (Table 3). APM: absolute plate motion from the HS3-Nuvel-1A model [*Gripp and Gordon*, 2002] in the hotspot reference frame (white arrow). The domains are modified from *Toteu et al.* [2004] and *Nzenti et al.* [2006], YD: Yaounde Domain (Neoproterozoic); AYD: Adamawa-Yade Domain (Paleoproterozoic); and WCD: Western Cameroon Domain (Neoproterozoic). Heavy grey lines are major strike-slip faults associated with the CASZ as defined by *Ngako et al.* [2003], *Toteu et al.* [2004], and *Nzenti et al.* [2006]. SSZ: Sanaga Shear Zone and TBSZ: Tchollir-Banyo Shear Zone. Heavy dashed lines are thrust faults. The red line delineates the low-velocity zone at 200 km depth from the *P* wave tomographic model of *Reusch et al.* [2010].

Garoua rift in the north (Figure 1); (2) weak anisotropy ($\delta t \approx 0.3$ s) between the Congo Craton and the CVL; (3) N-S oriented fast polarization directions within the CVL, with $\delta t \approx 0.7$ s. In line with the findings of our study, *Koch et al.* [2012] found no evidence in support of complex patterns of anisotropy (e.g., dipping or multiple anisotropic layers). The main discrepancies between the *Koch et al.* [2012] study and ours are at stations CM01, CM03, CM09, CMC11, CM13, CM16, CM19, CM20, CM23, CM25, CM28, and CM30. Here the earlier study presents splitting parameters (ϕ, δt) that contrast with the null measurements we present. With the exception of CM28 and CM30, the δt observations resulting from the stacking methodology adopted by *Koch et al.* [2012] are extremely small at these stations, ranging from 0.28 to 0.53 s. Larger δt values at stations CM28 (1.05 ± 0.2 s) and CM30 (0.88 ± 0.04 s) contrast more significantly with our findings (Table 4).

5.2. Seismicity in Cameroon

During the 5 months analyzed, we located 203 local earthquakes with magnitudes ranging between 1.4 and 3 (Figure 8). The earthquakes are primarily concentrated near to Mount Cameroon (153 earthquakes), and the remainder are positioned offshore on the eastern side of Bioko (50 earthquakes). The rate of activity is variable with just 15 and 16 earthquakes reported for February and March 2006 respectively, increasing to 42 and 54 earthquakes in April and May 2006. Seventy-two earthquakes were reported for June 2006.

Table 3. Null Shear Wave Splitting Observations

Station	Station Lat/Lon (°N/°E)	BAZ (°)	Event Lat/Lon (°N/°E)
CM01	2.39/9.83	86.66	3.40/99.09
		94.90	−5.47/128.13
		22.87	51.15/157.52
CM02	2.70/13.29	30.78	46.47/153.24
		30.92	46.35/153.17
CM03	3.52/15.03	91.77	−3.08/129.44
		241.36	−28.72/−72.54
		242.75	−27.21/−71.06
		25.46	51.15/157.52
CM05	2.94/9.91	94.60	−5.47/128.13
CM07	3.87/11.46	61.97	25.32/123.36
		81.71	6.27/124.03
		29.58	46.35/153.17
		23.47	51.15/157.52
CM09	4.23/9.33	225.40	−44.87/−80.56
CM10	4.22/10.62	28.87	46.47/153.24
		29.01	46.35/153.17
		22.93	51.15/157.52
CM11	3.98/13.19	30.36	46.47/153.24
		24.39	51.15/157.52
CM12	4.48/11.63	86.80	1.07/126.28
		98.40	−9.05/110.36
CM13	4.59/9.46	93.70	−5.47/128.13
CM15	5.03/9.93	93.48	−5.47/128.13
CM16	5.48/10.57	28.51	46.47/153.24
		28.65	46.35/153.17
CM16	5.48/10.57	22.65	51.15/157.52
CM17	5.55/12.31	86.41	1.07/126.28
CM18	5.72/9.35	266.79	−3.29/−80.99
		27.75	46.47/153.24
		94.17	−6.53/129.93
		80.63	6.27/124.03
		93.07	−5.47/128.13
		27.88	46.35/153.17
		21.91	51.15/157.52
CM19	5.97/11.23	93.07	−5.47/128.13
		22.92	51.15/157.52
CM20	6.22/10.05	86.75	3.40/99.09
		92.85	−5.47/128.13
CM22	6.48/13.27	254.20	−15.59/−73.16
CM23	6.37/10.79	92.83	−5.47/128.13
CM24	6.52/14.29	264.47	−5.68/−76.40
		267.34	−3.29/−80.99
		277.01	6.86/−77.79
CM25	6.76/11.81	240.99	−28.72/−72.54
		92.73	−5.47/128.13
CM26	7.26/13.55	254.43	−15.35/−72.96
		54.08	31.02/130.00
CM28	8.47/13.24	64.20	22.87/121.28
		276.90	6.86/−77.79
		242.42	−27.21/−71.06
CM29	9.35/13.39	90.22	0.59/98.46
		29.16	46.47/153.24
		241.19	−28.72/−72.54
CM30	9.76/13.95	241.29	−28.72/−72.54
CM31	10.33/15.26	237.64	−31.75/−67.18
		28.87	47.28/154.15
CM32	10.62/14.37	29.43	46.47/153.24
		29.56	46.35/153.17
		242.60	−27.21/−71.06

Table 4. A Comparison of Shear Wave Splitting Parameters From This Study With That of *Koch et al.* [2012]

	This study				*Koch et al.* [2012]			
Station	ϕ(°)	σ_ϕ (deg)	δt (s)	$\sigma_{\delta t}$ (s)	ϕ (deg)	σ_ϕ (deg)	δt (s)	$\sigma_{\delta t}$ (s)
CM01	NULL				12	5	0.53	0.18
CM02	36	1	1.15	0.03	42	1	0.95	0.01
CM03	NULL				20	3	0.35	0.01
CM04	NO RESULT				47	3	0.60	0.05
CM05	19	9	0.60	0.14	22	3	0.70	0.06
CM06	42	1	0.98	0.04	56	1	0.78	0.01
CM07	NULL				NULL			
CM08	NO RESULT				25	3	1.10	0.04
CM09	NULL				26	9	0.43	0.10
CM10	28	4	0.65	0.04	42	3	0.75	0.05
CM11	NULL				21	3	0.25	0.04
CM12	2	1	1.95	0.09	7	3	0.78	0.08
CM13	NULL				11	12	0.45	0.16
CM14	NO RESULT				−32	3	0.35	0.05
CM15	47	16	0.48	0.13	9	1	1.00	0.09
CM16	NULL				26	4	0.28	0.04
CM17	30	4	1.65	0.11	26	2	1.33	0.04
CM18	NULL				NULL			
CM19	NULL				2	3	0.45	0.04
CM20	NULL				−1	3	0.48	0.07
CM21	73	4	1.50	0.08	56	1	0.70	0.05
CM22	62	4	0.80	0.07	72	1	1.10	0.01
CM23	NULL				−15	2	0.53	0.05
CM24	76	4	0.75	0.13	46	4	0.30	0.05
CM25	NULL				−15	2	0.53	0.05
CM26	57	4	0.63	0.06	74	3	0.63	0.01
CM27	38	12	0.78	0.13	44	8	0.43	0.09
CM28	NULL				15	7	1.05	0.20
CM29	63	1	1.15	0.03	57	1	0.93	0.04
CM30	NULL				57	4	0.88	0.04
CM31	64	2	0.88	0.09	44	4	0.95	0.06
CM32	52	2	0.93	0.05	41	4	0.83	0.08

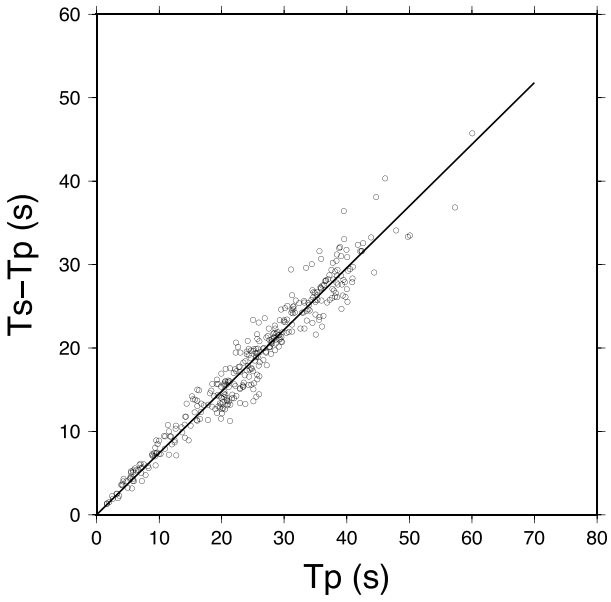

Figure 6. Wadati diagram showing the difference between *S* and *P* wave traveltimes versus *P* wave traveltime. The best fit line corresponds to a V_p/V_s ratio of 1.74.

In contrast to previous studies that utilized seismic data only from stations located around Mount Cameroon, our study draws upon data from seismic stations located along the full length of the CVL. Most of the line is aseismic with activity confined to the region around Mount Cameroon and Bioko (Figure 6).

Earthquakes near Mount Cameroon are distributed throughout the crust, with the majority ≤10 km deep; eight lower crustal earthquakes occurred at 20–35 km depth (Figures 7 and 8a). The shallow earthquakes form two main groups, with the majority forming a NNE-SSW striking, ~40 km long cluster ~40 km east of Mount Cameroon, close to an inferred major CASZ fault. A second cluster, ~15 km long on the northern flank of Mount Cameroon is subparallel to faults that define the NW-SE striking Bokosso graben. Lower crustal

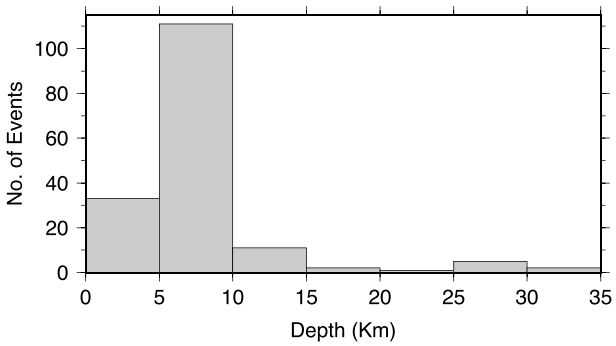

Figure 7. The depth distribution of earthquakes in Cameroon along the continental sector of the CVL. Earthquakes with depth uncertainties larger than ±2 km are not plotted.

earthquakes are located beneath the east and south flanks of Mount Cameroon within ~20 km of the summit. Fifty earthquakes located in the Gulf of Guinea, mostly to the east of Bioko, define a ~20 km wide, ~80 km long cluster striking NNE-SSW (Figure 8).

The distribution of earthquakes in our study is broadly similar to that reported during continuous seismic monitoring in 1985–1992 following the 1982 eruption of Mount Cameroon. At that time, seismic activity was mainly in the upper crust beneath the Bokosso graben, and in distinct clusters 40 km south, 40 km east, and 10–20 km southeast of Mount Cameroon [*Ambeh and Fairhead*, 1991; *Ubangoh et al.*, 1997; *Ateba and Ntepe*, 1997]. The latter cluster had earthquakes in the lower crust, as in our study, but also extending to 65 km depth, within the mantle lithosphere [*Ambeh and Fairhead*, 1991].

The rate of seismicity we report is toward the low end of that observed during 1985–1992. Our values are comparable to the 3–4 earthquakes per 10 days reported during 1991 and 1992, but lower than the ≤60 per 10 days reported during 1986, 1988, and in 1990 [*Ubangoh et al.*, 1997]. Importantly, however, our new results show that the first-order pattern of seismic activity that characterized Mount Cameroon during 1985–1992 persisted until 2006, except that we do not find significant seismicity beneath the summit of Mount Cameroon, as was observed during summit eruptions in 1999 and 2000 [*Ateba et al.*, 2009].

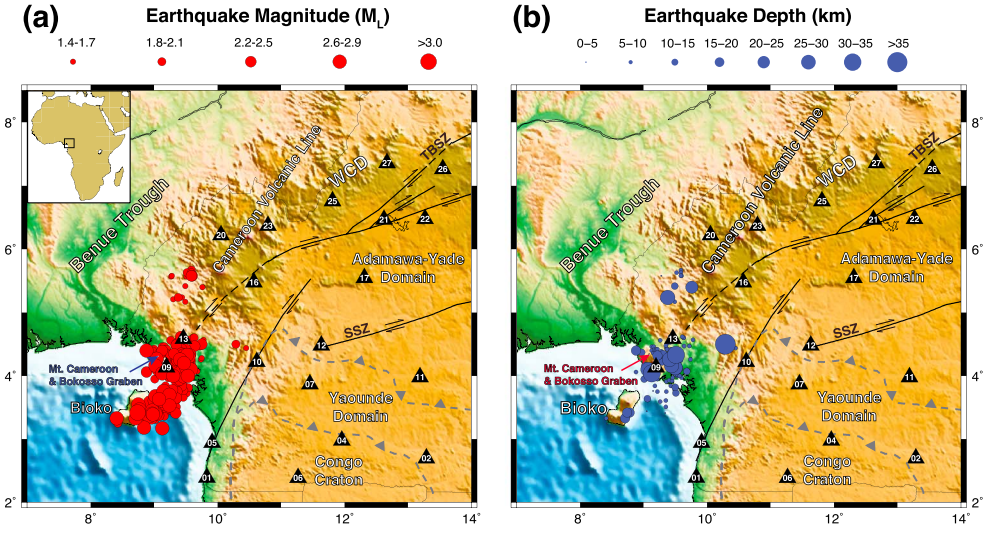

Figure 8. Seismicity along the CVL during February–May 2006. (a) Local earthquake magnitudes and (b) local earthquake depths in Cameroon. Heavy dashed lines are thrust faults. The domains are modified from *Toteu et al.* [2004] and *Nzenti et al.* [2006]. WCD: Western Cameroon Domain (Neoproterozoic). Heavy black lines are major strike-slip faults of the Central African Shear Zone. SSZ: Sanaga Shear Zone. Black numbered triangles are seismograph station locations.

6. Discussion

In this section, we use the results of our seismicity and *SKS* splitting studies to address outstanding questions concerning the reasons for the development of the CVL and the nature of the magmatic plumbing system beneath it.

6.1. Seismicity Along the CVL

Our analysis of seismicity demonstrates that earthquake activity is focused on and around Mount Cameroon, the most recently active volcano of the CVL. This suggests a strong link between spatially localized magmatic processes and the generation of brittle failure in the crust. A notable feature of our results is the presence of lower crustal earthquakes at 20–35 km depth beneath the south and east flanks of the volcano (Figures 7 and 8). Earthquakes of similar depth have been reported beneath Icelandic volcanoes such as Eyjafjallajokull and Askja [*Tarasewicz et al.*, 2012; *Key et al.*, 2011], beneath rift valley flank volcanoes in East Africa [e.g., *Keir et al.*, 2009], and beneath intraplate volcanoes related to hotspots such as Kilauea volcano in Hawaii [e.g., *Wolfe et al.*, 2003]. Although we cannot preclude the possibility that this deformation is the result of localized deep crustal faulting beneath the CVL, the association between deep earthquakes and crustal magmatism in these studies suggests that brittle failure of the lower crust may be the result of elevated strain rates, induced by the flow of magma or the release of volatiles from the magma.

Upper crustal seismicity is identified on a fault system subparallel to the CASZ to the east of Mount Cameroon; it is also identified beneath the Bokosso graben, which is oriented orthogonal to the CASZ (Figure 8). Similar to the lower crustal seismicity, the shallow earthquakes are characterized by emergent phase arrivals and relatively low frequency content (<4 Hz), again pointing toward the migration of magma or magma-derived volatiles through crustal fracture networks [e.g., *Chouet and Matoza*, 2013]. Mount Cameroon last erupted 6 years before the time period of our study and the preexisting fault systems delineated by shallow earthquakes are not associated with magmatism. We thus favor the interpretation that the seismicity was induced by migration of pressurized volatiles, released during cooling of localized intrusions deeper in the lithosphere. This interpretation is supported by field measurements of ongoing gas release from the CASZ to the south and southeast of Mount Cameroon, coincident with the location of earthquakes [*Ubangoh et al.*, 1997; *Turner et al.*, 2013]. Gas release was also observed in 1907 on the NE flank of the volcano, as well as at the summit in 1861 [*Ubangoh et al.*, 1997].

Away from Mount Cameroon, the lack of seismic and volcanic activity (Figure 8) suggests that there is little evidence for active magma chambers and magma supply routes along the western sector of the CVL, consistent with the view that magmatism is dominated by low-volume alkaline basaltic volcanism, with associated short crustal residence times [e.g., *Suh et al.*, 2003]. Supporting evidence comes from constraints of bulk crustal V_p/V_s ratios along the CVL, which are remarkably low (~1.74)[*Gallacher and Bastow*, 2012], with the implication that little mafic material is present at depth beneath the region, either as present-day melt, cooled gabbroic intrusions, or fractionated products of erupted lavas. The low V_p/V_s ratio observation from the *Gallacher and Bastow* [2012] receiver function study is corroborated by our seismicity data set (Figure 6). Oceanic intraplate shields such as Hawaii [e.g., *Leahy and Park*, 2005] and Galapagos [e.g., *Tepp et al.*, 2014] have V_p/V_s ~1.8, but the values we observe from Cameroon are markedly low when compared to other continental hotspots such as Ethiopia [e.g., *Daly et al.*, 2008], where large volumes of melt within the crust can push V_p/V_s ratios to ≥1.80. Spatially localized magmatism along the CVL is thus likely delivered episodically from directly beneath individual volcanic centers during decadal to century timescale periods of intrusions and eruptions with associated degassing activity.

In the following sections, we explore the extent to which our *SKS* splitting study can inform about the deformation history of the Cameroon lithosphere, the CVL's magmatic plumbing system, the mantle flow field beneath it, and the implications of our results for the development of the chain.

6.2. Causes of Seismic Anisotropy in Cameroon

Patterns of seismic anisotropy can develop due to the preferential alignment of minerals in the crust and/or mantle, the preferential alignment of fluid or melt, or some combination thereof [e.g., *Blackman and Kendall*, 1997]. A range of processes could lead to such anisotropy, including (1) asthenospheric flow parallel to absolute plate motion [e.g., *Vinnik et al.*, 1989; *Bokelmann*, 2002; *Assumpção et al.*, 2006], (2) mantle flow around the continental keel beneath the Congo Craton [e.g., *Fouch et al.*, 2000], and (3) a preexisting fossil anisotropy frozen in the lithosphere [e.g., *Silver and Chan*, 1988; *Vauchez and Nicolas*, 1991; *Bastow et al.*,

2011]. Estimates of the amount of splitting that can be accrued in the crust vary from 0.1–0.3 s [*Silver*, 1996] to 0.1–0.5 s [*Barruol and Mainprice*, 1993]. Thus, a mantle contribution is required to explain the observations at a number of stations in Cameroon. At 12 of the 14 stations where we draw a null conclusion, *Koch et al.* [2012] either also present a null or $\delta t \leq 0.53$ s (Table 4). These small δt values can likely be explained relatively easily with hypotheses concerning only the crust.

The direction of motion of the African Plate shows poor correlation with the ϕ values presented in Figure 5, thus ruling out basal drag as the principal cause of the observed anisotropy. Equally, there is little evidence in our results for lateral flow of asthenospheric material beneath the CVL. Our results therefore do not provide conclusive support for the hypothesis of *Ebinger and Sleep* [1998] that flow of buoyant asthenosphere beneath continental lithosphere thinned extensively during Mesozoic rifting may now be contributing to volcanism along the CVL. Laterally extensive horizontal asthenospheric flow patterns due to plate motions or mantle flow in the region would, using Fresnel zone arguments [e.g., *Alsina and Snieder*, 1995], be expected to produce only gradual variations in ϕ and δt across the network [e.g., *Forte et al.*, 2010]. However, we cannot preclude the possibility that a narrow, focused asthenospheric flow channel exists beneath the region, to which our splitting study is insensitive.

If the CVL had experienced plate stretching during the opening of the South Atlantic, as was the case for the Benue Trough to the NW of our network, the lithosphere might be expected to have inherited an olivine lattice preferred orientation (LPO) fabric parallel to the approximately NW-SE oriented extension direction [e.g., *Vinnik et al.*, 1992; *Gao et al.*, 1997]. Alternatively, in hotspots such as Ethiopia, patterns of anisotropy are attributed to rift parallel-oriented melt pockets in the lithosphere [e.g., *Kendall et al.*, 2006; *Bastow et al.*, 2010]. The observations from Cameroon are not so easily explained by either of these mechanisms because much of the CVL is characterized by null measurements (Figure 5 and Table 3), and the larger values of δt are found away from regions characterized by low mantle seismic wave speeds and Cenozoic volcanism (e.g., CM02 on the Congo Craton; Figure 5).

One potential reason for the apparent lack of melt in the CVL lithosphere compared to Ethiopia may be the considerably greater degree of focused tectonic faulting and fracturing in Ethiopia [e.g., *Hayward and Ebinger*, 1996], which enhances focused magmatism along strike in the rift [*Ebinger and Casey*, 2001; *Rooney et al.*, 2011]. Additionally, decompression melting in response to extension is expected to enhance melt volume production in Ethiopia compared to Cameroon, where there is no evidence for present-day extension. Thus, while we cannot preclude the possibility that poorly aligned, stationary melt exists in the lithosphere beneath the CVL, our study yields no evidence for significant magmatic extension beneath the CVL nor is there any evidence for strongly aligned melt along CASZ faults/fractures.

The null measurements we observe beneath much of the CVL (Figure 5 and Table 3) may be indicative of a widespread vertical LPO fabric beneath much of the region, with the *a* axis of the mantle olivine crystals perpendicular to the particle motion of our near vertically propagating *SKS* phases. If true, this latter flow direction would be consistent with hypotheses for the development of the CVL that include either a mantle plume or the upwelling limb of a small-scale convection cell beneath the region [e.g., *Morgan*, 1983; *Burke*, 2001; *Reusch et al.*, 2010]. Predictions of LPO mantle seismic anisotropy from tomography-based models of mantle convection [*Forte et al.*, 2010] also suggest a strong vertical component to the mantle flow field beneath Cameroon, consistent with our observations. The same study also predicts a horizontal flow component, however, for which our results do not provide compelling evidence. Alternatives to the isotropic or vertical flow field hypotheses exist though, not least the possibility that our back azimuthal event coverage is insufficient to characterize anisotropic fabrics beneath the stations we classify here as null. Plastic deformation of peridotites usually results in the alignment of the (100) axis of olivine parallel to the direction of flow [e.g., *Zhang and Karato*, 1995; *Bystricky et al.*, 2000; *Tommasi et al.*, 2000]; however, the apparent isotropy inferred from our *SKS* splitting analysis could also result from a horizontal flow field in the event that olivine crystallographic orientations have axial *b* patterns [e.g., *Vauchez et al.*, 2005; *Bascou et al.*, 2008]. Null observations could also be the result of a two-layered model with orthogonal fast directions as has been suggested, for example, at station CAN in Australia [*Barruol and Hoffmann*, 1999].

Splitting parameters, where observed in Cameroon, vary over length scales of ~100 km (e.g., CM40–CM32; Figure 5), thus implying a relatively shallow anisotropic layer in some regions of the study area: a deep source of anisotropy would produce only subtle variations across the network. Lithospheric thickness is ~100 km beneath the CVL, but as much as ~250 km thick beneath the Congo Craton [e.g., *Fishwick*, 2010].

Thus, in the following sections we explore the hypothesis that fossil lithospheric fabrics exist beneath some parts of Cameroon.

6.3. Fossil Lithospheric Anisotropy in Cameroon

Although there is some debate as to whether or not tectonic processes in the Archean were capable of imparting a seismic anisotropic fabric on the lithosphere [e.g., *Fouch et al.*, 2004], younger Precambrian fabrics have been identified in many areas worldwide. For example, the thick lithosphere of northern Canada retains a strong fossil lithospheric fabric of the ~1.8 Ga Trans-Hudson Orogen [*Bastow et al.*, 2011], which marked the final stages of the assembly of Laurentia. Precambrian fossil lithospheric fabrics are also found, for example, in southern Africa [e.g., *Silver et al.*, 2001; *Fouch et al.*, 2004] and northern Europe (Fennoscandia) [e.g., *Plomerová and Babuska*, 2010]. Unlike Cameroon, these regions have since experienced no significant tectonic reworking.

Cameroon comprises several tectonic domains that span more than 3 Ga of the geological record, including the Archean Ntem Complex in southernmost Cameroon [e.g., *Tchameni et al.*, 2001], the Neoproterozoic Yaounde Domain [*Oliveira et al.*, 2006], and the Oubanguides Belt, which were assembled during the Pan-African Orogeny ~600 Ma (Figure 1). Our observations do not match the orientation of these terrane boundaries, however, thus indicating that a Precambrian fossil lithospheric fabric associated with Gondwana assembly is no longer present. At stations CM02, CM03, and CM06, for example, anisotropic fabrics are oblique to the trend of the suture between the Ntem Complex and Yaounde domains. Instead, ϕ values at these stations correspond more closely to the SW-NE trend of the CASZ. It is difficult to determine the extent of Mesozoic reworking in parts of Cameroon because surface geology is masked by dense rain forest. However, further north, where structural geological constraints are available [e.g., *Toteu et al.*, 2004; *Nzenti et al.*, 2006; *Ngako et al.*, 2003], anisotropic fast directions at stations CM17, CM21, CM22, CM24, CM26, and CM27 mirror the trends of the large-scale strike-slip faults that reactivated during the early stages of Gondwana breakup in Mesozoic times (Figure 5). In the northernmost part of the study area, anisotropic fast directions at stations CM29, CM31, and CM32 are also likely related to shear zones in the lithosphere, with apparently little influence from the obliquely (~N125°E) trending Garoua rift. Narrow pull-apart basins along the CASZ in Cameroon might have resulted in the development of anisotropic strain fabrics perpendicular to those seen in Figure 5 and have thus not resulted in the same lithospheric-scale deformation as the strike-slip faults.

A striking observation in Figure 5 is the abundance of null measurements along the CVL, below which mantle seismic wave speeds are known to be relatively slow [*Reusch et al.*, 2010]. Our study thus yields no evidence for a well-preserved fossil lithospheric fabric beneath much of the CVL. The Mesozoic reactivation of the CASZ is known to have affected this region in the form of strike-slip faulting, but we observe no evidence for the well-defined lithospheric anisotropic fabrics seen elsewhere in Cameroon. One possible explanation for this is that hotspot activity during both the breakup of Gondwana and the subsequent development of the CVL has destroyed the older fossil lithospheric fabrics. Hotspot tectonism associated with the Mesozoic opening of the South Atlantic ~130 Ma may have thermomechanically eroded Precambrian age fossil lithospheric fabrics beneath the CVL, though its thermal influence would have long since dissipated and the lithosphere rethickened. To some extent, the lithosphere may have remained relatively thin on account of ongoing small-scale convection between the two-flanking cratons. The new, thin lithosphere would have been expected to inherit a new fossil anisotropic signature during cooling. However, anisotropic basal drag fabrics do not develop easily during slow absolute plate motion [e.g., *Debayle and Ricard*, 2013] as is observed for present-day Cameroon. The young lower lithosphere of the CVL may thus not have inherited a new fossil anisotropic signature. On the other hand, studies of mantle seismic anisotropy from the Ronda Massif in Spain [*Vauchez et al.*, 2005] and from Polynesia [*Tommasi et al.*, 2004] conclude that fossil fabrics are inherited from older deformation and that partial melting and melt percolation under static conditions cannot erase preexisting olivine crystal preferred orientations. Thus, we cannot completely preclude the possibility that the apparent lack of fossil lithospheric fabrics beneath the western end of the continental CVL is simply the result of inadequate data coverage in our study. The null observations could also be the result of a two-layer model with orthogonal fast directions [e.g., *Barruol and Hoffmann*, 1999]. Either way, the paucity of melt in the CVL lithosphere implied by both our seismicity and *SKS* splitting studies certainly does not support the view that metasomatism has greatly modified the lithosphere, at least during the past 30 Ma.

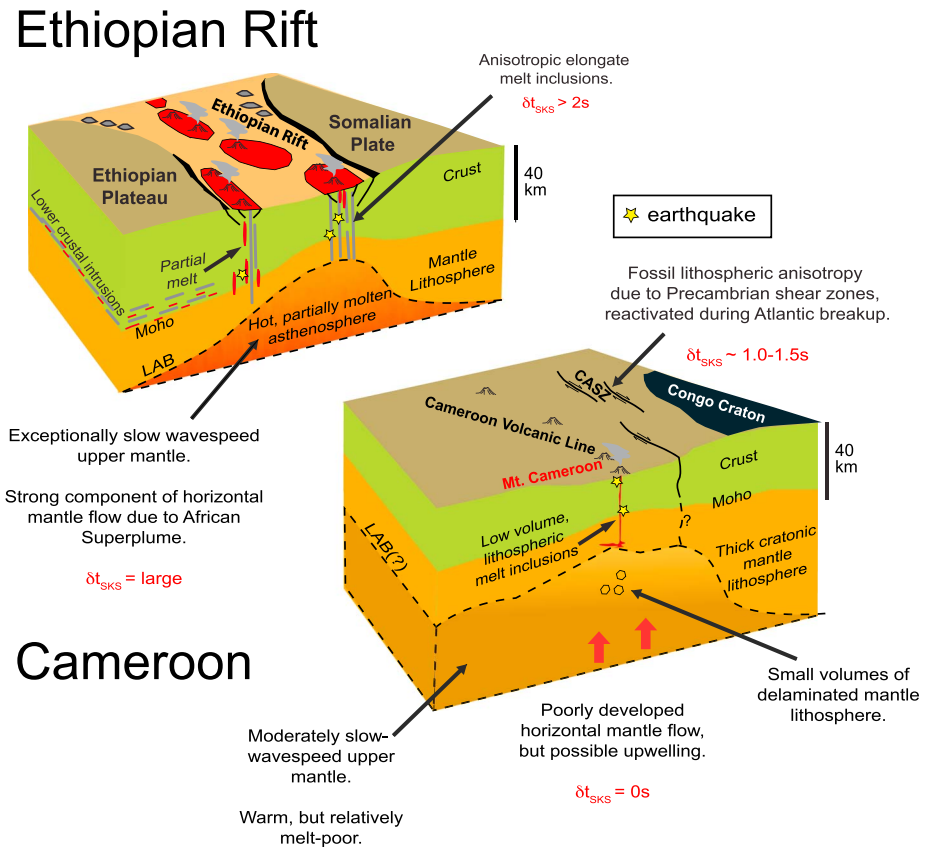

Figure 9. A summary conceptual cartoon for the Cameroon crust and mantle compared to that in the magmatically active Ethiopian rift. LAB: lithosphere-asthenosphere boundary; CASZ: Central African Shear Zone; and δt_{SKS}: the splitting delay time observed in *SKS* phases. Modified after *Gallacher and Bastow* [2012].

6.4. Implications for the Origins of the CVL

While our study is not able to discriminate unambiguously between many of the competing hypotheses for the development of the CVL (e.g., plume versus small-scale convection), an actively upwelling component of mantle flow seems plausible beneath the CVL. The lack of evidence for aligned melt in the lithosphere, however—a common feature at other hotspots such as Ethiopia [e.g., *Kendall et al.*, 2006; *Bastow et al.*, 2010; *Keir et al.*, 2011]—is consistent with the findings of petrological studies that indicate only minimal fractionation of magmas within the shallow lithosphere prior to rapid eruption [*Fitton and Dunlop*, 1985; *Fitton*, 1987; *Marzoli et al.*, 2000; *Déruelle et al.*, 2007; *Suh et al.*, 2003]. Our local earthquake traveltime data set reveals the CVL crust has a low V_p/V_s ratio (1.74; Figure 8), an observation in agreement with teleseismic receiver function studies of bulk crustal structure [*Gallacher and Bastow*, 2012] that also provides little evidence for large-scale modification of the crust beneath the CVL. The sporadic development of alkaline basaltic volcanism in Cameroon over the past ~30 Ma may thus be explained better by lower melt volume hypotheses such as shear zone reactivation [e.g. *Fairhead*, 1988] or lithospheric instabilities at the edge of continents [e.g., *Milelli et al.*, 2012].

Recent work by *Milelli et al.* [2012] and *Fourel et al.* [2013] used scaled laboratory models and analytical solutions to investigate the effects of large lateral variations in lithospheric thickness on lithospheric stability. Their work demonstrates that lithospheric instabilities can develop over long timescales with small rates of upwelling and decompression melting as is observed in Cameroon. Over time, removal of small volumes of lithosphere beneath the CVL would be expected to erode the CASZ-related fossil anisotropic fabrics observed elsewhere in Cameroon. In between delamination events, new lithosphere formed by conductive plate cooling might be expected to inherit a new LPO anisotropic fabric, but Africa's very slow movement NW since ~30 Ma [e.g., *Steinberger and Torsvik*, 2008] may mean that basal drag fabrics beneath the CVL are minimal and the new lithosphere thus assumes a near-isotropic seismic signature. Figure 9

illustrates schematically how the CVL's magmatic plumbing system and underlying mantle flow field compares to those observed beneath the Ethiopian hotspot province, which is superposed by a mature rift zone, in contrast to the CVL.

7. Conclusions

We have performed seismicity and *SKS* splitting studies of the Cameroon Volcanic Line (CVL) with a view to understanding better the tectonic/geodynamic processes responsible for its development. The seismicity study indicates the region is markedly less seismically active than other continental intraplate hotspot worldwide, with little evidence for magmatism-related crustal deformation away from Mount Cameroon, which last erupted in 2000. The local earthquake traveltime data set reveals low crustal V_p/V_s ratios of ~1.74, which match earlier receiver function-derived values for the bulk crust in Cameroon [*Gallacher and Bastow*, 2012].

The *SKS* splitting study yields no evidence for strongly aligned anisotropic melt inclusions beneath the CVL, as observed at some hotspots elsewhere. Instead, anisotropic fast polarization directions in Cameroon, where observed, parallel the Precambrian Central African Shear Zone (CASZ). However, along the western continental portion of the CVL, only null splitting measurements are found. We cannot completely preclude the possibility that this is the result of two anisotropic layers with orthogonal fast directions. Alternatively, the nulls may imply the CVL asthenosphere is isotropic or characterized by a vertically oriented olivine LPO fabric due, perhaps, to a mantle plume, or the upward limb of a small-scale convection cell between the Congo and West African Cratons. Precambrian CASZ fossil anisotropic fabrics along the CVL may have been thermomechanically eroded during the Mesozoic breakup of Gondwana (~130 Ma), with an isotropic lower lithosphere subsequently reforming thermally during the slow movement of the African plate. Small-scale lithospheric delamination during the 30 Ma recent development of the line may also have contributed to the erosion of the lithosphere beneath the CVL. This would have served both to erode CASZ fossil anisotropic fabrics and to generate the spatially and temporally sporadic low-volume alkaline basaltic volcanism observed along the line (Figure 9).

Acknowledgments
The CBSE network was operated by Pennsylvania State University. Data from the CBSE network were all sourced freely from the IRIS Data Management Center (DMC) http://www.iris.edu/dms/nodes/dmc. We thank G. Helffrich, M. Kendall, J. Di Leo, K. Cashman, L. Caricchi, and S. Sparks for helpful discussions about Cameroon. Insightful reviews from C. Ebinger and A. Tommasi greatly improved the contribution. R.G. is supported by a NERC studentship. I.B. is funded by the Leverhulme Trust. This work was partially funded by Natural Environment Research Council grant number NE/K500926/1.

References

Alsina, D., and R. Snieder (1995), Small-scale sublithospheric mantle deformation: Constraints from SKS splitting observations, *Geophys. J. Int.*, *123*, 431–448.

Ambeh, W., and J. Fairhead (1991), Regular, deep seismicity beneath Mt Cameroon volcano: Lack of evidence for tidal triggering, *Geophys. J. Int.*, *106*(1), 287–291.

Assumpção, M., M. Heintz, A. Vauchez, and M. Silva (2006), Upper mantle anisotropy in SE and central Brazil from SKS splitting: Evidence of asthenospheric flow around a cratonic keel, *Earth Planet. Sci. Lett.*, *250*(1–2), 224–240, doi:10.1016/j.epsl.2006.07.038.

Ateba, B., and N. Ntepe (1997), Post-eruptive seismic activity of Mount Cameroon (Cameroon), West Africa: A statistical analysis, *J. Volcanol. Geotherm. Res.*, *79*(1–2), 25–45.

Ateba, B., C. Dorbath, L. Dorbath, N. Ntepe, M. Frogneux, J. Delmond, and D. Manguelle (2009), Eruptive and earthquake activities related to the 2000 eruption of Mount Cameroon volcano (West Africa), *J. Volcanol. Geotherm. Res.*, *179*(3–4), 206–216, doi:10.1016/j.jvolgeores.2008.11.021.

Barruol, G., and R. Hoffmann (1999), Upper mantle anisotropy beneath the Geoscope stations, *J. Geophys. Res.*, *104*(B5), 10,757–10,773, doi:10.1029/1999JB900033.

Barruol, G., and D. Mainprice (1993), A quantitative evaluation of the contribution of crustal rocks to the shear-wave splitting of teleseismic SKS waves, *Phys. Earth Planet. Int.*, *78*, 281–300.

Bascou, J., G. Delpech, A. Vauchez, B. Moine, J. Cottin, and G. Barruol (2008), An integrated study of microstructural, geochemical, and seismic properties of the lithospheric mantle above the Kerguelen plume (Indian Ocean), *Geochem. Geophys. Geosyst.*, *9*(4), Q04036, doi:10.1029/2007GC001879.

Bastow, I., T. Owens, G. Helffrich, and J. Knapp (2007), Spatial and temporal constraints on sources of seismic anisotropy: Evidence from the Scottish highlands, *Geophys. Res. Lett.*, *34*(5), L05305, doi:10.1029/2006GL028911.

Bastow, I., S. Pilidou, J.-M. Kendall, and G. Stuart (2010), Melt-induced seismic anisotropy and magma assisted rifting in Ethiopia: Evidence from surface waves, *Geochem. Geophys. Geosyst.*, *11*, Q0AB05, doi:10.1029/2010GC003036.

Bastow, I., D. Thompson, J. Wookey, J. Kendall, G. Helffrich, D. Snyder, D. Eaton, and F. Darbyshire (2011), Precambrian plate tectonics: Seismic evidence from northern Hudson Bay, Canada, *Geology*, *39*(1), 91–94, doi:10.1130/G31396.1.

Blackman, D., and J.-M. Kendall (1997), Sensitivity of teleseismic body waves to mineral texture and melt in the mantle beneath a mid-ocean ridge, *Phil. Trans. R. Soc. Lond.*, *355*, 217–231.

Bokelmann, G. (2002), Which forces drive North America?, *Geology*, *30*(11), 1027–1030.

Burke, K. (2001), Origin of the Cameroon line of volcano-capped swells, *J. Geol.*, 349–362.

Bystricky, M., K. Kunze, L. Burlini, and J.-P. Burg (2000), High shear strain of olivine aggregates: Rheological and seismic consequences, *Science*, *290*(5496), 1564–1567.

Castaing, C., J. Feybesse, D. Thiéblemont, C. Triboulet, and P. Chèvremont (1994), Palaeogeographical reconstructions of the Pan-African/Brasiliano orogen: Closure of an oceanic domain or intracontinental convergence between major blocks?, *Precambrian Res.*, *69*(1–4), 327–344.

Chouet, B., and R. Matoza (2013), A multi-decadal view of seismic methods for detecting precursors of magma movement and eruption, *J. Volcanol. Geotherm. Res.*, *252*, 108–175, doi:10.1016/j.jvolgeores.2012.11.013.
Daly, E., D. Keir, C. Ebinger, G. Stuart, I. Bastow, and A. Ayele (2008), Crustal tomographic imaging of a transitional continental rift: The Ethiopian rift, *Geophys. J. Int.*, *172*(3), 1033–1048, doi:10.1111/j.1365-246X.2007.03682.x.
Daly, M., J. Chorowicz, and J. Fairhead (1989), Rift basin evolution in Africa: The influence of reactivated steep basement shear zones, in *Inversion Tectonics*, vol. 44, edited by M. A. Cooper and G. D. Williams, pp. 309–334, Geol. Soc. Spec. Pub., London, doi:10.1144/GSL.SP.1989.044.01.17.
Debayle, E., and Y. Ricard (2013), Seismic observations of large-scale deformation at the bottom of fast-moving plates, *Earth Planet. Sci. Lett.*, *376*, 165–177, doi:10.1016/j.epsl.2013.06.025.
Déruelle, B., I. Ngounouno, and D. Demaiffe (2007), The Cameroon Hot Line (CHL): A unique example of active alkaline intraplate structure in both oceanic and continental lithospheres, *Comptes Rendus Geosci.*, *339*(9), 589–600.
Djomani, Y., J. Nnange, M. Diament, C. Ebinger, and J. Fairhead (1995), Effective elastic thickness and crustal thickness variations in West Central Africa inferred from gravity data, *J. Geophys. Res.*, *100*(B11), 22,047–22,070, doi:10.1029/95JB01149.
Dorbath, C., L. Dorbath, J. Fairhead, and G. Stuart (1986), A teleseismic delay time study across the Central African shear zone in the Adamawa region of Cameroon, West Africa, *Geophys. J. R. Astr. Soc.*, *86*(3), 751–766.
Dugda, M., A. Nyblade, and J. Julià (2007), Thin lithosphere beneath the Ethiopian plateau revealed by a joint inversion of Rayleigh wave group velocities and receiver functions, *J. Geophys. Res.*, *112*, B08305, doi:10.1029/2006JB004918.
Ebinger, C., and M. Casey (2001), Continental breakup in magmatic provinces: An Ethiopian example, *Geology*, *29*, 527–530.
Ebinger, C., and N. Sleep (1998), Cenozoic magmatism throughout East Africa resulting from impact of a single plume, *Nature*, *395*, 788–791.
Ebinger, C., A. Ayele, D. Keir, J. Rowland, G. Yirgu, T. Wright, M. Belachew, and I. Hamling (2010), Length and timescales of rift faulting and magma intrusion: The Afar rifting cycle from 2005 to present, *Ann. Rev. Earth Planet. Sci.*, *38*, 439–466.
Fairhead, J. (1988), Mesozoic plate tectonic reconstructions of the Central South Atlantic Ocean: The role of the West and Central African rift system, *Tectonophysics*, *155*(1–4), 181–191.
Fairhead, J., and R. Binks (1991), Differential opening of the Central and South Atlantic oceans and the opening of the West African rift system, *Tectonophysics*, *187*(1–3), 191–203.
Fairhead, J., and C. Okereke (1987), A regional gravity study of the West African rift system in Nigeria and Cameroon and its tectonic interpretation, *Tectonophysics*, *143*(1–3), 141–159.
Ferguson, D., J. Maclennan, I. Bastow, D. Pyle, S. Jones, D. Keir, J. Blundy, T. Plank, and G. Yirgu (2013), Melting during late-stage rifting in Afar is hot and deep, *Nature*, *499*(7456), 70–73, doi:10.1038/nature12292.
Fishwick, S. (2010), Surface wave tomography: Imaging of the lithosphere-asthenosphere boundary beneath Central and Southern Africa?, *Lithos*, *120*(1–2), 63–73.
Fishwick, S., and I. Bastow (2011), Towards a better understanding of African Topography, a review of passive-source seismic studies of the African crust and upper mantle, in *The Formation and Evolution of Africa: A Synopsis of 3.8 Ga of Earth History*, vol. 357, edited by D. Van Hinsbergen et al., pp. 343–371, Geol. Soc. Lond. Spec. Pub., London, doi:10.1144/SP357.19.
Fitton, J. (1980), The Benue Trough and Cameroon Line—A migrating rift system in West Africa, *Earth Planet. Sci. Lett.*, *51*(1), 132–138.
Fitton, J. (1987), The Cameroon line, West Africa: A comparison between oceanic and continental alkaline volcanism, in *Alkaline Igneous Rocks*, vol. 30, edited by J. G. Fitton and B. G. J. Upton, pp. 273–291, Geol. Soc. Lond. Spec. Pub., London, U. K.
Fitton, J., and H. Dunlop (1985), The Cameroon Line, West Africa, and its bearing on the origin of oceanic and continental Alkali Basalt, *Earth Planet. Sci. Lett.*, *72*(1), 23–38.
Forte, A., R. Moucha, N. Simmons, S. Grand, and J. Mitrovica (2010), Deep-mantle contributions to the surface dynamics of the North American continent, *Tectonophysics*, *481*, 3–15, doi:10.1016/j.tecto.2009.06.010.
Fouch, M., A. Fischer, E. Parmentier, M. Wysession, and T. Clarke (2000), Shear wave splitting, continental keels, and patterns of mantle flow, *J. Geophys. Res.*, *105*, 6255–6276, doi:10.1029/1999JB900372.
Fouch, M., P. Silver, D. Bell, and J. Lee (2004), Small-scale variations in seismic anisotropy near Kimberley, South Africa, *Geophys. J. Int.*, *157*, 764–774, doi:10.1111/j.1365-246X.2004.02234.x.
Fourel, L., L. Milelli, C. Jaupart, and A. Limare (2013), Generation of continental rifts, basins, and swells by lithosphere instabilities, *J. Geophys. Res. Solid Earth*, *118*, 3080–3100, doi:10.1002/jgrb.50218.
Gallacher, R., and I. Bastow (2012), The development of magmatism along the Cameroon Volcanic Line: Evidence from teleseismic receiver functions, *Tectonics*, *31*, TC3018, doi:10.1029/2011TC003028.
Gao, S., P. Davis, H. Liu, P. Slack, A. Rigor, Y. Zorin, V. Mordvinova, V. Kozhevnikov, and N. Logatchev (1997), SKS splitting beneath the continental rift zones, *J. Geophys. Res.*, *102*, 22,781–22,797.
Gripp, A., and R. Gordon (2002), Young tracks of hotspots and current plate velocities, *Geophys. J. Int.*, *150*(2), 321–361, doi:10.1046/j.1365-246X.2002.01627.x.
Halliday, A., A. Dickin, A. Fallick, and J. Fitton (1988), Mantle Dynamics: A Nd, Sr, Pb and O Isotopic Study of the Cameroon Line Volcanic Chain, *J. Petrol.*, *29*(1), 181–211, doi:10.1093/petrology/29.1.181.
Hayward, N., and C. Ebinger (1996), Variations in the along–axis segmentation of the Afar rift system, *Tectonics*, *15*, 244–257.
Keir, D., G. Stuart, A. Jackson, and A. Ayele (2006), Local earthquake magnitude scale and seismicity rate for the Ethiopian Rift, *Bull. Seismol. Soc. Am.*, *96*(6), 2221–2230.
Keir, D., I. Bastow, K. Whaler, E. Daly, D. Cornwell, and S. Hautot (2009), Lower crustal earthquakes near the Ethiopian rift induced by magmatic processes, *Geochem. Geophys. Geosyst.*, *10*, Q0AB02, doi:10.1029/2009GC002382.
Keir, D., C. Pagli, I. Bastow, A. Ayele, and E. Ababa (2011), The magma-assisted removal of Arabia in Afar: Evidence from dike injection in the Ethiopian rift captured using InSAR and seismicity, *Tectonics*, *30*(2), TC2008, doi:10.1029/2010TC002785.
Kendall, J.-M., S. Pilidou, D. Keir, I. Bastow, G. Stuart, and A. Ayele (2006), Mantle upwellings, melt migration and the rifting of Africa: Insights from seismic anisotropy, in *The Afar Volcanic Province within the East African Rift System*, vol. 259, edited by G. Yirgu, C. J. Ebinger, and P. K. H. Maguire, pp. 271–293, Geol. Soc. Lond. Spec. Pub., London, U. K.
Keranen, K., S. Klemperer, J. Julia, J. Lawrence, and A. Nyblade (2009), Low lower crustal velocity across Ethiopia: Is the main Ethiopian Rift a narrow rift in a hot craton?, *Geochem. Geophys. Geosyst.*, *10*, Q0AB01, doi:10.1029/2008GC002293.
Key, J., R. White, H. Soosalu, and S. Jakobsdóttir (2011), Multiple melt injection along a spreading segment at Askja, Iceland, *Geophys. Res. Lett.*, *38*, L05301, doi:10.1029/2010GL046264.
King, S. (2007), Hotspots and edge-driven convection, *Geology*, *35*(3), 223, doi:10.1130/G23291A.1.
King, S., and D. Anderson (1998), Edge–driven convection, *Earth Planet. Sci. Lett.*, *160*, 289–296.

Klein, F. (2002), *User's Guide to HYPOINVERSE-2000: A Fortran Program to Solve for Earthquake Locations and Magnitudes*, pp. 1–123, Open-File Report 2002-171, U.S. Geological Survey, Menlo Park, Calif.

Koch, F., D. Wiens, A. Nyblade, P. Shore, R. Tibi, B. Ateba, C. Tabod, and J. Nnange (2012), Upper mantle anisotropy beneath the Cameroon Volcanic Line and Congo Craton from shear wave splitting measurements, *Geophys. J. Int.*, *190*, 75–86, doi:10.1111/j.1365-246X.2012.05497.x.

Leahy, G., and J. Park (2005), Hunting for oceanic island Moho, *Geophys. J. Int.*, *160*(3), 1020–1026.

Lee, D., A. Halliday, J. Fitton, and G. Poli (1994), Isotopic variations with distance and time in the volcanic islands of the Cameroon Line: Evidence for a mantle plume origin, *Earth Planet. Sci. Lett.*, *123*(1–3), 119–138.

Lowry, A., and M. Pérez-Gussinyé (2011), The role of crustal quartz in controlling Cordilleran deformation, *Nature*, *471*(7338), 353–357.

Maguire, P., G. R. Keller, S. L. Klemperer, G. D. Mackenzie, K. Keranen, S. Harder, B. O'Reilly, H. Thybo, L. Asfaw, M. A. Khan, and M. Amha (2006), Crustal structure of the northern Main Ethiopian Rift from the EAGLE controlled-source survey; a snapshot of incipient lithospheric break-up, in *The Afar Volcanic Province Within the East African Rift System*, vol. 259, edited by G. Yirgu, C. J. Ebinger, and P. K. H. Maguire, pp. 269–291, Geol. Soc. Spec. Pub., London, U. K.

Marzoli, A., E. Piccirillo, P. Renne, G. Bellieni, M. Iacumin, J. Nyobe, and A. Tongwa (2000), The Cameroon Volcanic Line revisited: Petrogenesis of continental basaltic magmas from lithospheric and asthenospheric mantle sources, *J. Petrol.*, *41*(1), 87–109.

Meyers, J., B. Rosendahl, G. Harrison, and Z.-D. Ding (1998), Deep–imaging seismic and gravity results from the offshore Cameroon Volcanic Line, and speculation of African hotlines, *Tectonophysics*, *284*, 31–63.

Milelli, L., L. Fourel, and C. Jaupart (2012), A lithospheric instability origin for the Cameroon Volcanic Line, *Earth Planet. Sci. Lett.*, *335-336*, 80–87, doi:10.1016/j.epsl.2012.04.028.

Montelli, R., G. Nolet, F. Dahlen, and G. Masters (2006), A catalogue of deep mantle plumes: New results from finite-frequency tomography, *Geochem. Geophys. Geosyst.*, *7*, Q11007, doi:10.1029/2006GC001248.

Montigny, R., I. Ngounouno, and B. Deruelle (2004), Âges KAr des roches magmatiques du fossé de Garoua (Cameroun): Leur place dans le cadre de la Ligne du Cameroun, *Comptes Rendus Geosci.*, *336*(16), 1463–1471.

Morgan, J. (1983), Hotspot tracks and the early rifting of the Atlantic, *Tectonophysics*, *94*(1–4), 123–139.

Ngako, V., P. Affaton, J. Nnange, and T. Njanko (2003), Pan-African tectonic evolution in Central and Southern Cameroon: Transpression and transtension during sinistral shear movements, *J. Afr. Earth Sci.*, *36*(3), 207–214.

Ngako, V., E. Njonfang, F. Aka Tongwa, P. Affaton, and J. Nnange Metuk (2006), The North-South Paleozoic to quaternary trend of alkaline magmatism from Niger-Nigeria to Cameroon: Complex interaction between hotspots and precambrian faults, *J. Afr. Earth Sci.*, *45*(3), 241–256.

Nzenti, J., B. Kapajika, G. Wörner, and T. Lubala (2006), Synkinematic emplacement of granitoids in a Pan-African shear zone in Central Cameroon, *J. Afr. Earth Sci.*, *45*(1), 74–86.

Oliveira, E., S. Toteu, M. Araújo, M. Carvalho, R. Nascimento, J. Bueno, N. McNaughton, and G. Basilici (2006), Geologic correlation between the Neoproterozoic Sergipano Belt (NE Brazil) and the Yaoundé Belt (Cameroon, Africa), *J. Afr. Earth Sci.*, *44*(4–5), 470–478.

Pasyanos, M., and A. Nyblade (2007), A top to bottom lithospheric study of Africa and Arabia, *Tectonophysics*, *444*(1–4), 27–44.

Pérez-Gussinyé, M., M. Metois, M. Fernández, J. Vergés, J. Fullea, and A. Lowry (2009), Effective elastic thickness of Africa and its relationship to other proxies for lithospheric structure and surface tectonics, *Earth Planet. Sci. Lett.*, *287*(1–2), 152–167.

Plomerová, J., and V. Babuska (2010), Long memory of mantle lithosphere fabric—European LAB constrained from seismic anisotropy, *Lithos*, *120*(1), 131–143, doi:10.1016/j.lithos.2010.01.008.

Plomerova, J., V. Babuška, C. Dorbath, L. Dorbath, and R. Lillie (1993), Deep lithospheric structure across the Central African shear zone in Cameroon, *Geophys. J. Int.*, *115*(2), 381–390.

Poudjom Djomani, Y., M. Diament, and Y. Albouy (1992), Mechanical behaviour of the lithosphere beneath the Adamawa Uplift (Cameroon, West Africa) based on gravity data, *J. Afr. Earth Sci.*, *15*(1), 81–90.

Poudjom Djomani, Y., M. Diament, and M. Wilson (1997), Lithospheric structure across the Adamawa Plateau (Cameroon) from gravity studies, *Tectonophysics*, *273*(3–4), 317–327.

Priestley, K., D. McKenzie, E. Debayle, and S. Pilidou (2008), The African upper mantle and its relationship to tectonics and surface geology, *Geophys. J. Int.*, *175*(3), 1108–1126.

Rankenburg, K., J. Lassiter, and G. Brey (2005), The role of continental crust and lithospheric mantle in the Genesis of Cameroon Volcanic Line Lavas: Constraints from isotopic variations in Lavas and Megacrysts from the Biu and Jos Plateaux, *J. Petrol.*, *46*(1), 169–190.

Restivo, A., and G. Helffrich (1999), Teleseismic shear wave splitting measurements in noisy environments, *Geophys. J. Int.*, *137*, 821–830.

Reusch, A., A. Nyblade, D. Wiens, P. Shore, B. Ateba, C. Tabod, and J. Nnange (2010), Upper mantle structure beneath Cameroon from body wave tomography and the origin of the Cameroon Volcanic Line, *Geochem. Geophys. Geosyst.*, *11*, Q10W07, doi:10.1029/2010GC003200.

Reusch, A., A. Nyblade, R. Tibi, D. Wiens, P. Shore, A. Bekoa, C. Tabod, and J. Nnange (2011), Mantle transition zone thickness beneath Cameroon: Evidence for an upper mantle origin for the Cameroon Volcanic Line, *Geophys. J. Int.*, *187*(3), 1146–1150, doi:10.1111/j.1365-246X.2011.05239.x.

Richter, C. (1935), An instrumental earthquake magnitude scale, *Bull. Seismol. Soc. Am.*, *25*(1), 1–32.

Ritsema, J., A. Deuss, H. van Heijst, and J. Woodhouse (2011), S40RTS: A degree-40 shear-velocity model for the mantle from new Rayleigh wave dispersion, teleseismic traveltime and normal-mode splitting function measurements, *Geophys. J. Int.*, *184*(3), 1223–1236, doi:10.1111/j.1365-246X.2010.04884.x.

Rooney, T., I. Bastow, and D. Keir (2011), Insights into extensional processes during magma assisted rifting: Evidence from aligned scoria cones, *J. Volcanol. Geotherm. Res.*, 83–96, doi:10.1016/j.jvolgeores.2010.07.019.

Rooney, T., C. Herzberg, and I. Bastow (2012), Elevated mantle temperature beneath East Africa, *Geology*, *40*, 27–30, doi:10.1130/G32382.1.

Silver, P. (1996), Seismic anisotropy beneath the continents, *Annu. Rev. Earth Planet. Sci.*, *24*, 385–432.

Silver, P., and G. Chan (1991), Shear wave splitting and subcontinental mantle deformation, *J. Geophys. Res.*, *96*(B10), 16,429–16,454.

Silver, P., and W. Chan (1988), Implications for continental structure and evolution from seismic anisotropy, *Nature*, *335*(6185), 34–39.

Silver, P., and M. Savage (1994), The interpretation of shear wave splitting parameters in the presence of two anisotropic layers, *Geophys. J. Int.*, *119*, 949–963.

Silver, P., S. Gao, and K. Liu (2001), Mantle deformation beneath Southern Africa, *Geophys. Res. Lett.*, *28*, 2493–2496.

Sleep, N., C. Ebinger, and J.-M. Kendall (2002), Deflection of mantle plume material by cratonic keels, *J. Geol. Soc. Lond.*, *199*, 135–150.

Steinberger, B., and T. Torsvik (2008), Absolute plate motions and true polar wander in the absence of hotspot tracks, *Nature*, *452*(7187), 620–623, doi:10.1038/nature06824.

Stuart, G., J. Fairhead, L. Dorbath, and C. Dorbath (1985), Crustal structure of the Adamawa Plateau Cameroon, *Sci. Tech. Rev.*, *1*(1-2), 25–35.

Suh, C., S. Ayonghe, R. Sparks, C. Annen, J. Fitton, R. Nana, and A. Luckman (2003), The 1999 and 2000 eruptions of Mount Cameroon: Eruption behaviour and petrochemistry of lava, *Bull. Volcanol.*, *65*(4), 267–281.

Tadjou, J., R. Nouayou, J. Kamguia, H. Kande, and E. Manguelle-Dicoum (2009), Gravity analysis of the boundary between the Congo Craton and the Pan-African Belt of Cameroon, *Austrian J. Earth Sci.*, *102*(1), 71–79.

Tarasewicz, J., R. White, A. Woods, B. Brandsdóttir, and M. Gudmundsson (2012), Magma mobilization by downward-propagating decompression of the Eyjafjallajökull volcanic plumbing system, *Geophys. Res. Lett.*, *39*, L19309, doi:10.1029/2012GL053518.

Tchameni, R., K. Mezger, N. Nsifa, and A. Pouclet (2001), Crustal origin of early proterozoic syenites in the Congo Craton (Ntem Complex), South Cameroon, *Lithos*, *57*(1), 23–42.

Teanby, N., J.-M. Kendall, and M. Van der Baan (2004), Automation of shear-wave splitting measurements using cluster analysis, *Bull. Seismol. Soc. Am.*, *94*(2), 453–463.

Tepp, G., C. Ebinger, M. Ruiz, and M. Belachew (2014), Imaging rapidly deforming ocean island volcanoes in the western Galápagos archipelago, Ecuador, *J. Geophys. Res. Solid Earth*, *119*, 442–463, doi:10.1002/2013JB010227.

Thybo, H., and C. Nielsen (2009), Magma-compensated crustal thinning in continental rift zones, *Nature*, *457*, 873–876, doi:10.1038/nature07688.

Tokam, A., C. Tabod, A. Nyblade, J. Julià, D. Wiens, and M. Pasyanos (2010), Structure of the crust beneath Cameroon, West Africa, from the joint inversion of Rayleigh wave group velocities and receiver functions, *Geophys. J. Int.*, *183*(2), 1061–1076.

Tommasi, A., D. Mainprice, G. Canova, and Y. Chastel (2000), Viscoplastic self-consistent and equilibrium-based modeling of olivine lattice preferred orientations: Implications for the upper mantle seismic anisotropy, *J. Geophys. Res.*, *105*(B4), 7893–7908, doi:10.1029/1999JB900411.

Tommasi, A., M. Godard, G. Coromina, J. Dautria, and H. Barsczus (2004), Seismic anisotropy and compositionally induced velocity anomalies in the lithosphere above mantle plumes: A petrological and microstructural study of mantle xenoliths from French Polynesia, *Earth Planet. Sci. Lett.*, *227*(3), 539–556.

Toteu, S., J. Penaye, and Y. Djomani (2004), Geodynamic evolution of the Pan-African Belt in Central Africa with special reference to Cameroon, *Can. J. Earth Sci.*, *41*(1), 73–85.

Turner, M., M. Reagan, S. Turner, R. Sparks, H. Handley, G. Girard, and C. Suh (2013), Timescales of magma degassing-insights from U-series disequilibria, Mount Cameroon, West Africa, *J. Volcanol. Geotherm. Res.*, *262*, 38–46, doi:10.1016/j.jvolgeores.2013.06.003.

Ubangoh, R., B. Ateba, S. Ayonghe, and G. Ekodeck (1997), Earthquake swarms of Mt Cameroon, West Africa, *J. Afr. Earth Sci.*, *24*(4), 413–424.

Van Houten, F. (1983), Sirte Basin, north-central Libya: Cretaceous rifting above a fixed mantle hotspot?, *Geology*, *11*(2), 115–118.

Vauchez, A., and A. Nicolas (1991), Mountain building: Strike-parallel motion and mantle anisotropy, *Tectonophysics*, *185*(3), 183–201.

Vauchez, A., F. Dineur, and R. Rudnick (2005), Microstructure, texture and seismic anisotropy of the lithospheric mantle: Insights from the Labait volcano xenoliths (Tanzania), *Earth Planet. Sci. Lett.*, *232*, 295–314.

Vinnik, L., V. Farra, and B. Romanowicz (1989), Azimuthal anisotropy in the Earth from observations of SKS at Geoscope and NARS broadband stations, *Bull. Seismol. Soc. Am.*, *79*(5), 1542–1558.

Vinnik, L., L. Makeyeva, A. Milev, and A. Usenko (1992), Global patterns of azimuthal anisotropy and deformation in the continental mantle, *Geophys. J. Int.*, *111*, 433–447.

Wolfe, C., P. Okubo, and P. Shearer (2003), Mantle fault zone beneath Kilauea volcano, Hawaii, *Science*, *300*(5618), 478–480, doi:10.1126/science.1082205.

Zhang, S., and S.-I. Karato (1995), Lattice preferred orientation of olivine aggregates deformed in simple shear, *Nature*, *375*, 774–777.